

Single-site dissipation stabilizes a superconducting nonequilibrium steady state in a strongly correlated lattice

X. Z. Zhang^{1,*}

¹College of Physics and Materials Science, Tianjin Normal University, Tianjin 300387, China

Can superconducting order be made an attractor of open-system dynamics? We answer this question in the affirmative by proposing a minimal dissipation-engineering protocol for the particle-hole symmetric Hubbard chain. We apply a rotated quantum jump, namely a locally rotated η -pair lowering operator, on as little as a single lattice site and show that the resulting Lindblad evolution pumps the system from the vacuum into a nonequilibrium steady state (NESS) with η -pair off-diagonal long-range order (ODLRO). In contrast to schemes that rely on extensive dissipation or cooling into low-temperature phases, here a strictly local dissipative seed is sufficient to induce macroscopic pairing coherence across the entire interacting lattice. We elucidate the underlying mechanism from three complementary perspectives: the local dark-state structure of the rotated jump, strong-coupling protection of the holon-doublon manifold, and a Liouvillian symmetry/invariant-subspace picture that exposes the attractive fixed point and its spectral gap. We further show that the η -paired NESS is robust against a broad class of static disorder, which mainly modifies transients and relaxation rates, while identifying specific perturbations that dephase the pseudospin coherence and suppress long-range order. Our results establish a disorder-tolerant route to stabilizing superconducting order as a nonequilibrium attractor via minimal, local quantum-jump engineering.

I. INTRODUCTION

The paradigm of quantum state engineering has shifted fundamentally in recent years: rather than treating dissipation solely as a mechanism of decoherence, it is increasingly viewed as a resource for autonomous state preparation and stabilization[1–9]. By engineering the coupling between a system and its environment, one can design Liouvillian dynamics whose attractor (dark state) is a desired quantum many-body state[10–13]. This approach has successfully demonstrated the stabilization of entangled states[14–16], topological phases[17–20], and superfluid correlations[21–23] in various atomic, molecular, and optical (AMO) and solid-state platforms.

However, a major open challenge lies in extending these protocols to strongly correlated lattice systems where competing orders and constraints make the phase diagram fragile. Most existing schemes for stabilizing long-range order rely on spatially extensive dissipation—engineering reservoirs that couple to every site or bond of the lattice[7, 21]. While theoretically powerful, such bulk engineering is experimentally demanding and often incompatible with the natural local addressing capabilities of quantum devices. This raises a fundamental question of control and scalability: Is it possible to stabilize a macroscopic, strongly correlated quantum phase using only a minimal, strictly local dissipative seed?

In this work, we answer this question in the affirmative by demonstrating the dissipative stabilization of off-diagonal long-range order (ODLRO) in the Hubbard model using a single local dissipator. We focus on the paradigmatic setting of η -pairing superconductivity[24], an exact eigenstate phenomenon in the Hubbard model

that implies distance-independent pairing correlations protected by an SU(2) pseudospin symmetry. While η -pairing states are typically high-energy excited states in equilibrium and are thus thermodynamically unstable[25, 26], they represent ideal candidates for nonequilibrium steady states (NESS) if the appropriate dynamical symmetries can be enforced[27, 28].

We introduce a protocol based on a rotated quantum jump operator acting on as few as a single lattice site. Our results reveal a striking local-to-global mechanism: this local dissipative seed effectively pumps the entire interacting many-body system into a specific holon-doublon manifold, triggering a self-organization process that establishes global superconducting coherence. Crucially, this mechanism bypasses the need for bulk reservoir engineering. Instead, it exploits the interplay between the local dark-state structure enforced by the jump operator and the coherent Hamiltonian dynamics, which propagates the locally injected pseudospin coherence across the lattice.

Our analysis bridges the gap between the formal study of open-system symmetries and practical state preparation. Recent theoretical advances have clarified the role of strong and weak symmetries in determining the uniqueness and relaxation timescales of the NESS[29, 30]. Building on this, we show that our protocol leverages a dynamical selection rule that decouples the target superconducting manifold from competing dissipative decay channels. Furthermore, we address the critical issue of experimental realism by systematically investigating disorder. We identify a robust operational regime where the superconducting NESS and its ODLRO survive against a broad class of Hamiltonian perturbations, including static potential and interaction disorder, which are ubiquitous in solid-state and cold-atom experiments[31, 32].

The remainder of this paper is organized as follows. In Sec. II, we introduce the heuristic principle of rotated dis-

* zhangxz@tjnu.edu.cn

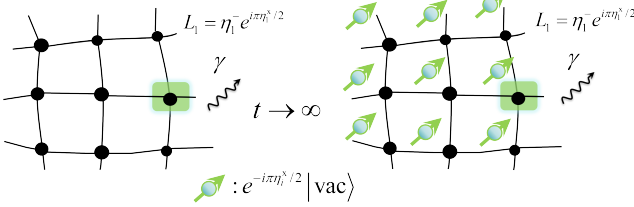


FIG. 1. Schematic of the nonequilibrium phase-locking protocol that stabilizes an η -paired superconducting NESS. Starting from a strongly correlated Hubbard system (with optional disorder in the interaction U_i , onsite potential μ_i , and/or bond hopping t_{ij}), we apply local rotated dissipation on selected sites with jump operators $L_j = \eta_j^- e^{i\frac{\pi}{2}\eta_j^x}$. Unlike the unrotated channel $\tilde{L}_j = \eta_j^-$, which simply annihilates pairs and leaves the vacuum as the local dark state, the rotation tilts the dissipative measurement axis so that the locally protected state is the $+y$ η -pseudospin eigenstate, $|\eta_j^y = +1/2\rangle \propto e^{-i\frac{\pi}{2}\eta_j^x}|0\rangle_j$, i.e., a coherent holon–doublon superposition. Each quantum jump then acts like a small compass correction: it damps misaligned components while repumping transverse η coherence. In the presence of strong correlations, this local axis selection propagates through the many-body dynamics, effectively phase-locking the η pseudospins across the lattice. At long times the system relaxes to a unique NESS with η pseudospins aligned along the $+y$ direction, yielding a finite η -pair amplitude and ODLRO.

sipation using a single-qubit toy model. Section III formalizes this intuition in the many-body Hubbard lattice, providing a rigorous analysis of the symmetry-protected subspaces and the Liouvillian spectrum that enables the local-to-global mechanism. In Sec. IV, we present numerical evidence for the dynamical emergence of η -pairing ODLRO, tracking the real-time evolution of pairing correlators. Section V presents a comprehensive study of robustness, classifying disorder into benign renormalization effects versus destructive symmetry-breaking perturbations. Finally, we summarize our findings and discuss outlooks for experimental realization in Sec. VI.

II. SINGLE-QUBIT HEURISTIC: ROTATED DISSIPATION PUMPS COHERENCE FROM THE VACUUM

We begin with the minimal open-system setting: a single spin-1/2 evolving under a Lindblad master equation

$$\dot{\rho} = \mathcal{L}\rho = -i[H, \rho] + L\rho L^\dagger - \frac{1}{2}\{L^\dagger L, \rho\}, \quad (1)$$

and set $H = 0$ throughout this section. The goal of this toy example is to make one mechanism completely transparent, in a form that will reappear in the Hubbard chain: a jump operator does not merely relax the system, it selects an attractive fixed point (a dark state or dark manifold). Consequently, by rotating the jump one rotates the dissipatively selected axis and therefore rotates

the steady state itself. In this way, dissipation can act as a simple coherence pump rather than a destroyer of phase information.

We first choose the standard (unrotated) lowering jump

$$L_0 = \sqrt{\gamma} s^-, \quad s^- = s^x - is^y. \quad (2)$$

Physically, this is the textbook amplitude-damping channel: population is irreversibly transferred from $|\uparrow\rangle$ to $|\downarrow\rangle$. Accordingly, $|\downarrow\rangle$ is a dark state since $L_0|\downarrow\rangle = 0$, and thus $\mathcal{L}(|\downarrow\rangle\langle\downarrow|) = 0$. Any initial state is driven toward the south pole of the Bloch sphere; in particular, the unique steady state has no transverse coherence.

To connect with the many-body construction below, it is useful to regard this spin-1/2 as a local pseudospin (the η -spin) on a Hubbard site, with the identification

$$|\downarrow\rangle \leftrightarrow |0\rangle, \quad |\uparrow\rangle \leftrightarrow |\uparrow\downarrow\rangle. \quad (3)$$

In this language, a transverse pseudospin polarization corresponds to a coherent superposition of the empty site $|0\rangle$ and the doublon $|\uparrow\downarrow\rangle$, and therefore to a nonzero onsite pairing amplitude $\langle\eta_i^+\rangle \neq 0$. The key question is then: can a purely dissipative operation select a steady state with such transverse coherence, starting from the local vacuum $|0\rangle$?

A minimal way is to rotate the jump. We consider

$$L(\theta) = \sqrt{\gamma} s^- e^{i\theta s^x}, \quad (4)$$

which can be viewed as applying the usual damping s^- in a locally rotated basis. Equivalently, the dissipator is engineered so that the dark state is no longer the south pole, but a state at a tunable latitude on the Bloch sphere. The special choice $\theta = \pi/2$ rotates the attractor onto the equator and thereby maximizes the transverse coherence. For a single jump channel, a pure steady state is most transparently obtained from the dark-state condition $L(\theta)|\psi_d\rangle = 0$. For $\theta = \pi/2$, $L_{\pi/2}|\psi_d\rangle = 0 \iff s^-(e^{i\frac{\pi}{2}s^x}|\psi_d\rangle) = 0 \iff e^{i\frac{\pi}{2}s^x}|\psi_d\rangle \propto |\downarrow\rangle$, and hence (see Appendix A for more details)

$$|\psi_d\rangle \propto e^{-i\frac{\pi}{2}s^x}|\downarrow\rangle = \frac{1}{\sqrt{2}}(|\downarrow\rangle - i|\uparrow\rangle). \quad (5)$$

This is the central point: the steady state is still a dark state of the jump, but it now lies on the equator of the Bloch sphere and therefore carries a finite transverse coherence,

$$\langle\psi_d|s^+|\psi_d\rangle = \frac{i}{2} \neq 0. \quad (6)$$

Equivalently, the steady-state Bloch vector points along $+\hat{y}$, with $\langle s^x \rangle = 0$ and $\langle s^y \rangle = 1/2$. Under the mapping (3), Eq. (6) is precisely the single-site analogue of $\langle\eta_i^+\rangle \neq 0$: the rotated dissipation does not “create coherence out of nothing”; rather, it reshapes the dark-state structure so that the unique attractor contains the desired coherence between $|0\rangle$ and $|\uparrow\downarrow\rangle$.

This local picture foreshadows the many-body mechanism exploited below. In the Hubbard chain, implementing the analogous rotated jump in the η -spin sector selects locally coherent holon–doublon superpositions as building blocks. The remaining task is to understand how interactions and hopping propagate and phase-lock this locally seeded η -pseudospin orientation across the lattice, resulting in an η -paired nonequilibrium steady state with off-diagonal long-range order.

III. SYMMETRY STRUCTURE, HOLON–DOUBLON PROTECTION, AND THE LIOUVILLIAN SPECTRUM

The single-qubit example shows that a rotated jump operator can reshape the local dark state and pump coherence along a chosen pseudospin direction. In the Hubbard setting, the same idea becomes nontrivial for two reasons: (i) the jump operators are local and therefore need not preserve global $SU(2)$ quantum numbers (in particular the global operator η^2), and (ii) the hopping term couples the holon–doublon sector to intermediate singly-occupied configurations. In this section we identify the dynamically relevant manifold, clarify which symmetries remain operative in the open system, and state the effective projected Liouvillian governing the long-time relaxation toward an η -paired NESS. A detailed derivation of the effective generator is provided in Appendix B.

A. Particle–hole symmetric Hubbard model and η - $SU(2)$

We consider the particle–hole symmetric Hubbard model on a bipartite lattice,

$$H_{\text{Hub}} = -t \sum_{\langle ij \rangle, \sigma} (c_{i\sigma}^\dagger c_{j\sigma} + \text{H.c.}) + U \sum_i \left(n_{i\uparrow} - \frac{1}{2} \right) \left(n_{i\downarrow} - \frac{1}{2} \right), \quad (7)$$

where half filling is enforced by the particle–hole symmetric interaction term. The model has the global $SO(4)$ symmetry $SO(4) \simeq SU(2)_S \times SU(2)_\eta / \mathbb{Z}_2$. Since our protocol targets pairing coherence, we focus on the η -pseudospin generators

$$\eta_i^\pm = \sum_i \eta_i^\pm, \quad (8)$$

$$\eta_i^+ = (-1)^i c_{i\uparrow}^\dagger c_{i\downarrow}^\dagger, \quad (9)$$

$$\eta_i^z = \frac{1}{2} (n_{i\uparrow} + n_{i\downarrow} - 1), \quad (10)$$

with $\eta_i^- = (\eta_i^+)^{\dagger}$ and $\eta_i^{x,y}$ defined in the standard way. They satisfy $[\eta_i^\alpha, \eta_j^\beta] = i\delta_{ij}\epsilon_{\alpha\beta\gamma}\eta_i^\gamma$. In the particle–hole

symmetric form (7), one has the strong commutation relations

$$[H_{\text{Hub}}, \eta^\pm] = 0, \quad [H_{\text{Hub}}, \eta^z] = 0, \quad (11)$$

and hence also $[H_{\text{Hub}}, \eta^2] = 0$.

B. Local rotated dissipation and the relevant invariant structure

We introduce rotated local jump operators acting on an arbitrary subset of sites $\mathcal{J} \subseteq \{1, \dots, N\}$,

$$L_j = \sqrt{\gamma} \eta_j^- e^{i\frac{\pi}{2}\eta_j^x} = \sqrt{\gamma} U_j^\dagger \eta_j^- U_j, \quad (12)$$

$$U_j = e^{-i\frac{\pi}{2}\eta_j^x}, \quad j \in \mathcal{J}. \quad (13)$$

The Lindblad evolution is

$$\partial_t \rho = \mathcal{L} \rho = -i[H_{\text{Hub}}, \rho] + \sum_{j \in \mathcal{J}} \left(L_j \rho L_j^\dagger - \frac{1}{2} \{L_j^\dagger L_j, \rho\} \right). \quad (14)$$

A key distinction from collective dissipation is that local L_j generally do not commute with the global operator $\eta^2 = (\sum_i \eta_i)^2$ because η^2 contains cross-terms $\sum_{k \neq \ell} \vec{\eta}_k \cdot \vec{\eta}_\ell$. Thus, in general,

$$[L_j, \eta^2] \neq 0, \quad (15)$$

and the open dynamics is not block-diagonal in global η sectors. This point is crucial for internal consistency: the $(N+1)$ -dimensional η -multiplet generated from the vacuum,

$$|\Psi_M\rangle \propto (\eta^+)^M |\text{vac}\rangle, \quad M = 0, 1, \dots, N, \quad (16)$$

is therefore not an exact invariant subspace of the full local-dissipative dynamics.

What is protected microscopically is the local representation structure of $\vec{\eta}_i$. The on-site Hilbert space decomposes into a singlet (singly-occupied) sector $\{|\uparrow\rangle_i, |\downarrow\rangle_i\}$ with $\eta_i = 0$ and a doublet (holon–doublon) sector $\{|\uparrow\rangle_i, |\downarrow\rangle_i\}$ with $\eta_i = \frac{1}{2}$. The local η_i^α act as spin-1/2 generators only within the doublet and annihilate the singlet. In particular,

$$\eta_i^\alpha |\uparrow\rangle_i = \eta_i^\alpha |\downarrow\rangle_i = 0, \quad L_i |\uparrow\rangle_i = L_i |\downarrow\rangle_i = 0. \quad (17)$$

Consequently, the dissipators themselves never create singlons. Starting from the fermionic vacuum $|\text{vac}\rangle = \bigotimes_i |\text{vac}\rangle_i$ (all sites in the $\eta_i = \frac{1}{2}$ doublet), the dissipative channel acts entirely within the tensor-product holon–doublon space

$$\mathcal{H}_{\text{HD}} = \bigotimes_{i=1}^N \text{span}\{|\text{vac}\rangle_i, |\uparrow\downarrow\rangle_i\}, \quad \dim \mathcal{H}_{\text{HD}} = 2^N. \quad (18)$$

However, the hopping term H_t does connect holon/doublon configurations to intermediate singly-occupied states and hence can generate virtual (and, away from strict limits, small but finite) excursions out of \mathcal{H}_{HD} .

C. Why the coherent generator drops out in the η -multiplet

Although $\mathcal{H}_\Psi = \text{span}\{|\Psi_M\rangle\}$ is not strictly invariant under local dissipation, it remains the natural slow sector for constructing an effective description because it is an exactly degenerate manifold of the particle–hole symmetric Hubbard Hamiltonian. Using (11) and the fact that the vacuum has zero energy in the particle–hole symmetric convention,

$$H_{\text{Hub}}|\text{vac}\rangle = 0, \quad (19)$$

one obtains for all M ,

$$H_{\text{Hub}}|\Psi_M\rangle = H_{\text{Hub}}(\eta^+)^M|\text{vac}\rangle = (\eta^+)^M H_{\text{Hub}}|\text{vac}\rangle = 0. \quad (20)$$

Therefore, for any operator ρ supported on \mathcal{H}_Ψ one has

$$-i[H_{\text{Hub}}, \rho] = 0. \quad (21)$$

Equivalently, in the doubled (ket \otimes bra) representation, the coherent contribution $-i(H_{\text{Hub}} \otimes \mathbb{I} - \mathbb{I} \otimes H_{\text{Hub}}^T)$ vanishes identically on $\mathcal{H}_\Psi \otimes \mathcal{H}_\Psi^*$. This observation motivates a degenerate projected effective theory on the doubled η -multiplet: the leading generator is obtained by projecting the dissipator onto $\mathcal{H}_\Psi \otimes \mathcal{H}_\Psi^*$. Because the local jumps do not conserve η^2 , this projection is not exact; rather, it is the first term in a controlled elimination of off-manifold components, in which both (i) intra-holon-doublon mixing among different global- η sectors induced by L_j and (ii) virtual leakage to singlons induced by H_t generate higher-order corrections. The resulting picture is fully consistent with the numerics: the attractive NESS is fixed already at leading order, while higher orders mainly renormalize transient relaxation pathways, which will show in the next section.

D. Leading projected Liouvillian, NESS, and the dissipative gap

Projecting the dissipator onto the doubled η -multiplet and using the η -SU(2) algebra yields the following leading effective generator (derived in Appendix B):

$$\hat{\mathcal{L}}_{\text{eff}}^{(0)} = -\frac{\gamma|\mathcal{J}|}{2} + \gamma \sum_{j \in \mathcal{J}} \left[\frac{1}{2} (\eta_j^y - \tilde{\eta}_j^y) + \eta_j^- e^{i\frac{\pi}{2}\eta_j^x} \tilde{\eta}_j^- e^{-i\frac{\pi}{2}\tilde{\eta}_j^x} \right], \quad (22)$$

where η_j ($\tilde{\eta}_j$) acts on the ket (bra) space. Importantly, Eq. (22) should be understood as a degenerate first-order projected Liouvillian on $\mathcal{H}_\Psi \otimes \mathcal{H}_\Psi^*$, not as the full microscopic generator for arbitrary parameters.

The steady state follows immediately. The rotated jump annihilates the local $+y$ eigenstate,

$$\eta_j^- e^{i\frac{\pi}{2}\eta_j^x} |\eta_j^y = +1/2\rangle = 0, \quad (23)$$

and therefore the product density matrix

$$\rho_{\text{ss}} = \bigotimes_{j=1}^N |\eta_j^y = +1/2\rangle \langle \eta_j^y = +1/2| \quad (24)$$

is a simultaneous dark state for any nonempty driven set \mathcal{J} . In particular,

$$|\langle \eta_i^+ \rangle_{\text{ss}}| = \frac{1}{2}, \quad |\langle \eta_i^+ \eta_j^- \rangle_{\text{ss}}| = \frac{1}{4} \quad (i \neq j), \quad (25)$$

consistent with the ODLRO of an η -paired condensate.

We finally address the relaxation timescale and robustness. The operator in (22) has a triangular structure in the η^y basis (Appendix C), implying that the eigenvalues are given by the diagonal entries and that the slowest nonzero decay rate is set by a single local y -pseudospin flip. This yields a leading dissipative gap

$$\Delta = \frac{\gamma}{2}. \quad (26)$$

The key physical point is that this gap is already present at the level of the projected generator, making ρ_{ss} a stable attractive fixed point. Deviations from the projected description arise from two distinct mechanisms: (i) intra-holon-doublon excursions in which local L_j mixes different global- η sectors within \mathcal{H}_{HD} , and (ii) leakage into the singlon sector mediated primarily by the hopping H_t . Both effects enter perturbatively through higher-order elimination of the off-manifold components and, in the parameter regime explored numerically, renormalize transient relaxation pathways without altering the observed NESS (24) or the dominant decay scale set by $\gamma/2$.

From the perspective of potential objections, three clarifications are useful. (i) *Effective gap and timescales*: Eq. (26) should be read as a property of the projected effective Liouvillian, namely that the leading-order reduced generator possesses a finite spectral separation scale set by the local pumping strength. In the full microscopic model, additional processes (e.g., hopping-assisted excursions and local sector mixing) renormalize relaxation pathways and can obscure a clean single-exponential rate extraction; rather than over-interpreting a fitted microscopic gap, we use $\Delta \sim \gamma/2$ as an organizing scale that captures why convergence remains rapid and why deviations are suppressed in the strong-coupling/controlled window where the effective elimination applies. (ii) *Finite-size scaling*: to separate genuine long-range order from finite-size saturation, we track the η -pair structure factor $S_\eta(\tau)$ as well as the global amplitude $|\Phi(\tau)|$ for increasing system sizes (Fig. 3); the weak size dependence of the steady-state plateaus supports an $\mathcal{O}(1)$ order parameter in the thermodynamic limit. (iii) *Uniqueness within the studied sector*: starting from the vacuum (holon–doublon) sector, the rotated jumps select a unique attractive fixed point in our simulations; in practice, the relevant question is not exact microscopic

invariance of the projected manifold, but whether off-manifold processes produce measurable steady-state deviations in accessible sizes and times, which they do not in the regime we consider.

IV. DYNAMICS: BUILDUP OF ODLRO AND CONVERGENCE TO AN η -PAIRED NESS

The central claim of this work is that the rotated local dissipation stabilizes a nonequilibrium superconducting steady state starting from the fermionic vacuum

$$|\text{vac}\rangle \equiv \bigotimes_{i=1}^N |0\rangle_i, \quad (27)$$

in the precise sense of off-diagonal long-range order (ODLRO) in the η -pair channel. This choice of initial state is essential: $|\text{vac}\rangle$ lies entirely in the holon–doublon doublet on every site and therefore provides a clean entry point for the dissipative pumping mechanism analyzed in Sec. II and the symmetry-based reduction of Sec. III. In particular, the protocol does not rely on fine-tuning a preformed paired state; rather, coherence is built up dynamically by the local jumps, which select a transverse η -pseudospin axis and actively phase-lock the system into an η -paired condensate.

To make this statement quantitative, we track two standard diagnostics of pairing coherence: (i) the one-point η -pair amplitude, which measures on-site holon–doublon coherence, and (ii) the real-space η -pair correlator as a function of separation, whose long-distance plateau constitutes the defining signature of ODLRO. Together, these observables provide a direct bridge between the single-spin pumping picture of Sec. II and the projected-Liouvillian analysis of Sec. III, and they allow us to verify explicitly that the long-time NESS exhibits superconducting order in the η -pair channel.

We diagnose pairing coherence using the local η -pair operator η_i^+ (and its Hermitian conjugate η_i^-). The local pairing amplitude,

$$\Phi_i(\tau) \equiv \langle \eta_i^+(\tau) \rangle, \quad \Phi(\tau) \equiv \frac{1}{N} \sum_{i=1}^N \langle \eta_i^+(\tau) \rangle, \quad (28)$$

directly measures the on-site coherence between $|0\rangle_i$ and $|\uparrow\downarrow\rangle_i$ (cf. the pseudospin mapping in Eq. (3)). To establish ODLRO we consider the two-point correlator

$$C_{ij}(\tau) \equiv \langle \eta_i^+(\tau) \eta_j^-(\tau) \rangle, \quad (29)$$

and, for periodic systems, its translationally averaged version

$$C(r, \tau) \equiv \frac{1}{N} \sum_{i=1}^N \langle \eta_i^+(\tau) \eta_{i+r}^-(\tau) \rangle. \quad (30)$$

ODLRO corresponds to a nonzero long-distance limit,

$$C_\infty(\tau) \equiv \lim_{r \rightarrow \infty} C(r, t) > 0, \quad (31)$$

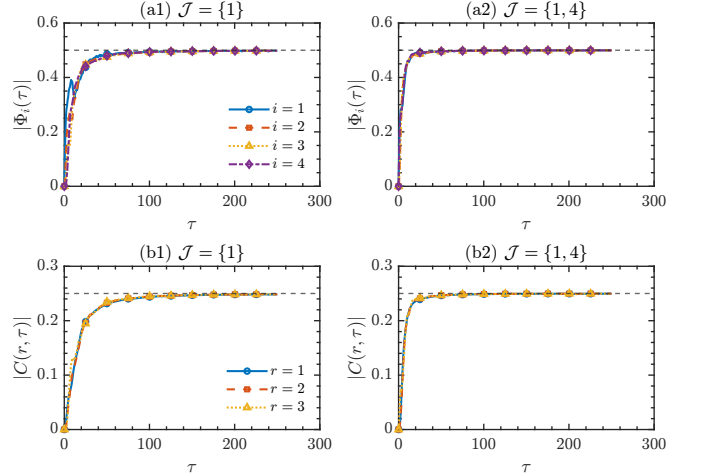


FIG. 2. Real-time buildup of η -pair coherence under open boundary conditions (OBC) for $N = 4$ at $t = \gamma$, $U = 8/\gamma$, and the rotation angle $\theta = \pi/2$. Top panels: site-resolved one-point amplitude $|\Phi_i(\tau)| = |\langle \eta_i^+(t) \rangle|$ for (a1) a single driven site $\mathcal{J} = \{1\}$ and (a2) two driven sites $\mathcal{J} = \{1, 4\}$; the dashed line indicates the projected benchmark $|\Phi_i| = 1/2$. Bottom panels: real-space profile of the two-point correlator magnitude $|C(r, \tau)| = |\langle \eta_i^+(t) \eta_{i+r}^-(t) \rangle|$ for multiple separations r (here $r = 1, 2, 3$), shown for (b1) $\mathcal{J} = \{1\}$ and (b2) $\mathcal{J} = \{1, 4\}$; the dashed line marks the predicted ODLRO plateau $|C| = 1/4$. At intermediate times short-range correlations develop first, while at late times the correlator becomes nearly independent of r and converges to an r -independent plateau $|C(r, t \rightarrow \infty)| \simeq 1/4$ (up to finite-size effects), providing direct evidence for ODLRO according to Eq. (31).

or, equivalently, to a finite η -pair structure factor

$$S_\eta(\tau) \equiv \frac{2}{N(N-1)} \sum_{i < j} \langle \eta_i^+(t) \eta_j^-(t) \rangle, \quad (32)$$

which remains $\mathcal{O}(1)$ in the thermodynamic limit.

At the level of the leading projected generator (22), the steady state is the product dark state (24), i.e., a local η -pseudospin polarization along $+y$ on every site. Equivalently, this NESS can be viewed as a coherent η -spin state obtained by rotating the trivial holon vacuum ($M = 0$) into the $+y$ direction:

$$|\text{NESS}\rangle = \bigotimes_{j=1}^N |\eta_j^y = +1/2\rangle \propto \exp\left(-i\frac{\pi}{2} \sum_{j=1}^N \eta_j^x\right) |\text{vac}\rangle, \quad (33)$$

so the long-time state is not built by Hamiltonian pairing but rather selected as a Lindbladian attractor by the rotated local jumps. This immediately implies the projected benchmarks

$$|\langle \eta_i^+ \rangle_{\text{ss}}| = \frac{1}{2}, \quad |\langle \eta_i^+ \eta_j^- \rangle_{\text{ss}}| = \frac{1}{4} \quad (i \neq j), \quad (34)$$

i.e. an ODLRO plateau $C_\infty = 1/4$ (up to finite-size corrections). Beyond the strictly projected picture, the

full microscopic evolution admits perturbative excursions outside the projected manifold. These arise from (i) intra-holon-doublon mixing among different global- η sectors induced by local L_j , and (ii) virtual leakage to singly occupied configurations mediated primarily by the hopping H_t . As discussed in Sec. III, such effects enter as higher-order corrections in the Schur-complement elimination of off-manifold components and predominantly renormalize transient relaxation pathways, while the leading attractive fixed point and the dominant decay scale $\Delta = \gamma/2$ [Eq. (26)] remain intact in the regime explored below.

We now verify these predictions by direct Lindblad time evolution and by computing $\langle O \rangle_\tau = \text{Tr}[\rho(\tau)O]$. Figures 2(a1) and (a2) show the time evolution of the local η -pair amplitude $|\Phi_i(\tau)| \equiv |\langle \eta_i^+ \rangle|$ and of a representative two-point correlator $|C(r, \tau)|$ for several choices of the driven set \mathcal{J} . In all cases the dynamics exhibits a rapid approach to the projected values, with $|\Phi_i(\tau \rightarrow \infty)| \rightarrow 1/2$ on a timescale governed by the dissipative gap. More importantly, Figures 2(b1) and (b2) display the full real-space profile $|C(r, \tau)|$ for multiple separations r , providing a direct visualization of the buildup of ODLRO. At intermediate times short-range correlations develop first, whereas at late times the correlator becomes nearly independent of r and converges to an r -independent plateau, $|C(r, \tau \rightarrow \infty)| \simeq 1/4$ for all $1 \leq r \leq N - 1$ (up to finite-size effects). This long-distance saturation constitutes direct evidence for ODLRO according to Eq. (31).

To further quantify the macroscopic order, we track the global amplitude $|\Phi(\tau)|$ and the structure factor $|S_\eta(\tau)|$; see Fig. 3. For dissipation applied only on the first site ($\mathcal{J} = \{1\}$), both observables rapidly approach steady plateaus that are essentially insensitive to system size (as N is increased), indicating that the observed order is not a finite-size artifact. In particular, the saturation of $|S_\eta(\tau)|$ to a finite plateau consistent with the real-space ODLRO limit provides a complementary, bulk-sensitive confirmation of the dissipatively stabilized η -paired NESS.

Before ending this part, we note that the resulting superconducting order is essentially a nonequilibrium phenomenon. The NESS does not emerge from thermalization under H_{Hub} : within the degenerate η -multiplet \mathcal{H}_Ψ , the Hamiltonian itself does not prefer a specific coherent orientation. Instead, the rotated local jumps act as a dissipative axis selector and continuously phase-lock the η pseudospins, making the ODLRO plateau an attractor of the open-system dynamics. This picture aligns with symmetry considerations: since the local dissipation generally breaks the global η^2 [Eq. (15)] symmetry, the steady state cannot be viewed as an equilibrium (or generalized-Gibbs) ensemble dictated by the conserved charges of H_{Hub} . Rather, ODLRO persists because it is actively stabilized by the driven dissipative dynamics, realizing a genuinely nonequilibrium η -paired steady state.

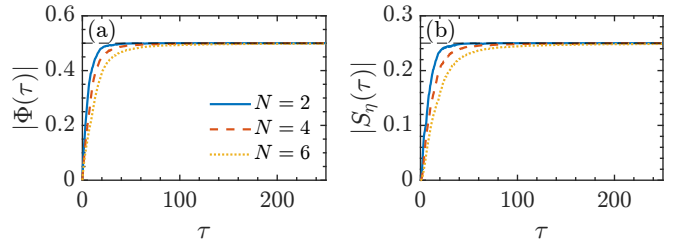


FIG. 3. Finite-size scaling of global η -pair order parameters for dissipation applied only on the first site $\mathcal{J} = \{1\}$. (a) Global η -pair amplitude $|\Phi(\tau)|$. (b) η -pair structure factor $|S_\eta(\tau)|$. Curves are shown for different system sizes (as labeled). Both observables rapidly approach steady plateaus that are essentially insensitive to N , indicating that the observed macroscopic order is not a finite-size artifact. In particular, the saturation of $|S_\eta(\tau)|$ to a finite value, consistent with the real-space long-distance ODLRO limit, provides a complementary, bulk-sensitive confirmation of the dissipatively stabilized η -paired NESS. Parameters: 1D chain, $t = \gamma$, $U = 4/\gamma$, and $\theta = \pi/2$.

V. DISORDER: STABILITY AND BREAKDOWN OF DISSIPATIVE η -PAIR ODLRO

Having established the dynamical buildup of η -pair coherence and the emergence of ODLRO in the clean system, we now address robustness: which microscopic imperfections leave the dissipatively prepared η -paired NESS essentially intact, and which disorders genuinely suppress (or destroy) the long-distance plateau? The answer is controlled by two closely related criteria: (i) whether the perturbation preserves the effective holon-doublon (HD) closure $\mathcal{H}_{\text{HD}} = \bigotimes_i \text{span}\{|0\rangle_i, |\uparrow\downarrow\rangle_i\}$ as an (approximately) closed dynamical sector, and (ii) within that sector, whether it competes with the dissipative pinning that selects a local pseudospin polarization along $+y$ direction.

To make the robustness statements operational (and easy to assess for finite systems), we focus on two complementary diagnostics in the steady state: the one-point amplitude $|\Phi_m|_{\text{ss}}$ and, more stringently, the long-distance correlator plateau $|C_m(r \rightarrow N/2)|_{\text{ss}}$. The latter directly probes the survival of ODLRO and is typically more sensitive to symmetry-breaking and leakage channels than local coherence. Throughout, we keep the rotated-jump channel fixed and introduce only static (quenched) perturbations in the Hamiltonian or in the jump parameters, so that the question is whether the NESS remains close to the clean $+y$ -polarized fixed point on the disorder-averaged level and across system sizes accessible to exact evolution.

A useful organizing principle, consistent with the discussion in Secs. III and IV, is that two distinct structures underlie the preparation protocol, and disorder can attack either one: (i) the local holon-doublon (HD) closure $\mathcal{H}_{\text{HD}} = \bigotimes_i \text{span}\{|0\rangle_i, |\uparrow\downarrow\rangle_i\}$, which is protected by the on-site η_i^2 algebra of the designed jump; and (ii) the

global slow manifold \mathcal{H}_Ψ (the doubled η -multiplet used for the triangular/gapped effective generator), which is the sector in which the coherent Hubbard contribution can be consistently eliminated to leading order. In the clean limit, these two mechanisms work together to produce an effectively classical pumping scenario: the rotated jump pins each local pseudospin along $+y$ direction, and the Liouvillian gap protects the late-time attraction to the product dark state.

We consider quenched disorder added to the microscopic Hubbard model,

$$H = H_{\text{Hub}} + H_{\text{dis}}, \quad (35)$$

while keeping the same rotated local jump operators $L_j = \sqrt{\gamma} \eta_j^- e^{i\frac{\pi}{2}\eta_j^x}$ on a chosen driven set. Numerically we quantify robustness by averaging over N_{dis} disorder realizations. For each disorder realization, we obtain the steady state either by evolving the Lindblad dynamics to the long-time limit or by directly solving for the zero eigenmode of the Liouvillian, and evaluate

$$|\Phi_m|_{\text{ss}} \equiv \frac{1}{N} \mathbb{E} \left| \sum_{i=1}^N \text{Tr}(\rho_{\text{ss}} \eta_i^+) \right|, \quad (36)$$

$$|C_m(r)|_{\text{ss}} \equiv \frac{1}{N} \mathbb{E} \left| \sum_{i=1}^N \text{Tr}(\rho_{\text{ss}} \eta_i^+ \eta_{i+r}^-) \right|, \quad (37)$$

where $\mathbb{E}[\dots]$ denotes the disorder average. In the ideal projected picture (Sec. III), the product dark state yields $|\langle \eta_i^+ \rangle_{\text{ss}}| = 1/2$ and $|\langle \eta_i^+ \eta_j^- \rangle_{\text{ss}}| = 1/4$ ($i \neq j$). Consequently, the most stringent test of robustness is whether a nonzero plateau $|C_m(r \rightarrow N/2)|_{\text{ss}} \approx 1/4$ persists in the long-distance limit.

A. Disorder with negligible impact on the η -paired NESS

We first discuss disorder types that, as protected by symmetry and confirmed numerically, leave the steady-state diagnostics essentially invariant (up to finite-size corrections), merely renormalizing transient relaxation rates. The defining feature of these perturbations is that they neither open direct leakage channels out of \mathcal{H}_{HD} nor generate coherent torques capable of overcoming the dissipative pinning scale set by the Liouvillian gap.

(i) *Interaction disorder.* We first consider randomness in the on-site interaction,

$$H_U = \sum_i \delta U_i \left(n_{i\uparrow} - \frac{1}{2} \right) \left(n_{i\downarrow} - \frac{1}{2} \right), \quad (38)$$

$$\delta U_i \in [U - W_U, U + W_U]. \quad (39)$$

This perturbation is diagonal in the local Fock basis and therefore does not, by itself, create matrix elements between the holon-doublon doublet $\{|0\rangle_i, |\uparrow\downarrow\rangle_i\}$ and the singlon states $\{|\uparrow\rangle_i, |\downarrow\rangle_i\}$. More importantly for our

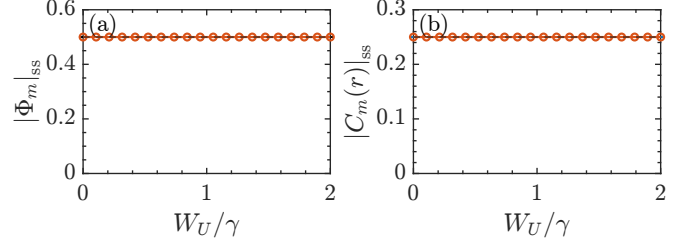


FIG. 4. Robustness against interaction disorder $U_i = U + \delta U_i$ as a function of W_U/γ . (a) $|\Phi_m|_{\text{ss}}$ and (b) $|C_m(r \rightarrow N/2)|_{\text{ss}}$. Points show disorder averages over 100 realizations; dashed lines mark the projected benchmarks $1/2$ and $1/4$. Parameters: 1D chain with PBC, $t = \gamma$, $U = 8/\gamma$, $\theta = \pi/2$, $N = 5$, and dissipation applied to site 1. Both correlators remain close to their projected values over the explored range of W_U/γ , indicating that the η -paired NESS is weakly affected by interaction inhomogeneity.

protocol, in the particle-hole symmetric convention the interaction term acts trivially within the holon-doublon manifold: on both $|0\rangle_i$ and $|\uparrow\downarrow\rangle_i$ one has

$$\left(n_{i\uparrow} - \frac{1}{2} \right) \left(n_{i\downarrow} - \frac{1}{2} \right) = \frac{1}{4}, \quad (40)$$

whereas on singlons it equals $-\frac{1}{4}$. Therefore, projecting onto the HD sector yields only an additive constant,

$$P_{\text{HD}} H_U P_{\text{HD}} = \sum_i \delta U_i \frac{1}{4} P_{\text{HD}} = \text{const.} \times P_{\text{HD}}, \quad (41)$$

i.e. interaction inhomogeneity does not generate an effective longitudinal η^z field nor any coherent precession within \mathcal{H}_{HD} (and hence within the projected doubled manifold).

As a result, U -disorder does not compete with the dissipative axis selection: it neither tilts the locally stabilized $+y$ dark direction nor enhances leakage out of the reduced manifold at leading order. The steady state selected by the rotated jumps is therefore unchanged. Consistent with this microscopic observation, our numerics show essentially no dependence of the NESS plateau values on the disorder strength W_U in the explored window: both $|\Phi_m|_{\text{ss}}$ and $|C_m(r \rightarrow N/2)|_{\text{ss}}$ remain pinned to the projected benchmarks $1/2$ and $1/4$ (up to finite-size fluctuations); see Fig. 4.

(ii) *Inhomogeneous dissipative strength.* We next consider inhomogeneous dissipation strengths,

$$L_j = \sqrt{\gamma_j} \eta_j^- e^{i\frac{\pi}{2}\eta_j^x}, \quad \gamma_j \in [\gamma - W_\gamma, \gamma + W_\gamma], \quad (42)$$

with the same rotated structure as in the clean protocol. Importantly, the local dark direction is independent of the pumping rate: for any $\gamma_j > 0$ the $+y$ -polarized pseudospin is annihilated, $L_j |\eta_j^y = +1/2\rangle = 0$. Therefore, γ -disorder does not shift the location of the attractive fixed point; it only redistributes the decay rates that govern the approach to it.

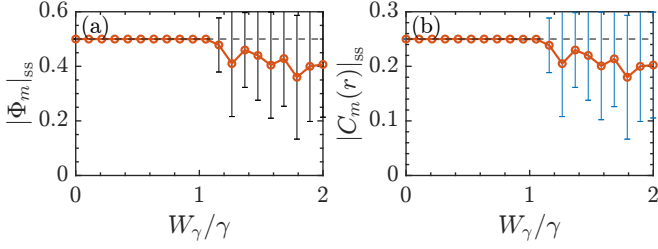


FIG. 5. Robustness against dissipation-strength disorder $\gamma_i = \gamma + \delta\gamma_i$ as a function of W_γ/γ . (a) $|\Phi_m|_{ss}$, and (b) $|C_m(r \rightarrow N/2)|_{ss}$. Points show disorder averages over 100 realizations; dashed lines mark the projected benchmarks 1/2 and 1/4. Parameters: 1D chain with PBC, $t = \gamma$, $U = 8/\gamma$, $\theta = \pi/2$, $N = 5$, and dissipation applied to site 1. Both correlators remain close to their projected values over a broad range of W_γ/γ , indicating that dissipative inhomogeneity weakly renormalizes the projected generator $\mathcal{L}_{\text{eff}}^{(0)}$. Error bars denote the standard error of the mean.

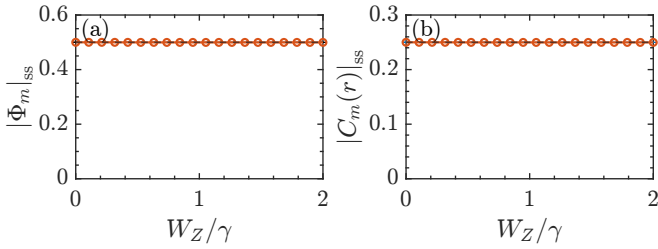


FIG. 6. Robustness against Zeeman-field disorder $B_i^z S_i^z + B_i^x S_i^x$ as a function of W_Z/γ . (a1) $|\Phi_m|_{ss}$, and (b1) $|C_m(r \rightarrow N/2)|_{ss}$. Points show disorder averages over 100 realizations; dashed lines mark the projected benchmarks 1/2 and 1/4. Parameters: 1D chain with PBC, $t = \gamma$, $U = 8/\gamma$, $\theta = \pi/2$, $N = 5$, and dissipation applied to site 1. Both correlators remain close to the projected values over the explored range of W_Z/γ , indicating that the η -paired NESS is only weakly affected by Zeeman inhomogeneity.

This redistribution has a transparent spectral consequence. In the projected picture each driven site contributes a local dissipative gap of order $\gamma_j/2$, so the slowest relaxation channel is controlled by the weakest pump, $\Delta_{\min} \sim \frac{1}{2} \min_{j \in \mathcal{J}} \gamma_j$. Hence, for moderate disorder where all γ_j remain appreciable, the NESS plateau values are essentially unchanged and only the transient dynamics becomes multi-rate (different sites lock to the $+y$ axis at different speeds). By contrast, once the distribution becomes broad enough that some γ_j are parametrically small (or approach zero when $W_\gamma \gtrsim \gamma$), the effective pinning gap no longer provides a uniform lower bound. In that regime, otherwise subleading processes, such as hopping-induced virtual excursions outside the reduced manifold, can operate over the long times set by $1/\Delta_{\min}$ and lead to visible deviations from the ideal η -paired plateau in finite systems. Numerically, this crossover occurs when W_γ becomes comparable to γ ; see Fig. 5.

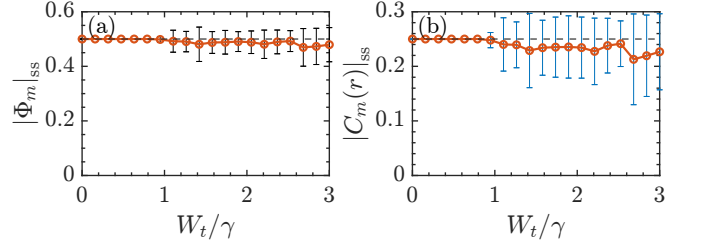


FIG. 7. Robustness against bond-disorder δt_{ij} as a function of W_t/γ . (a) $|\Phi_m|_{ss}$, and (b) $|C_m(r \rightarrow N/2)|_{ss}$. Points show disorder averages over 100 realizations; dashed lines mark the projected benchmarks 1/2 and 1/4. Parameters follow those in Fig. 6. In the perturbative window (large- U separation and/or Zeno pumping), bond-disorder-induced excursions into the singlon sector remain short-lived virtual processes and can be eliminated by a controlled Schur-complement expansion, resulting primarily in renormalized relaxation pathways within the reduced holon-doublon manifold. Consistently, both correlators stay pinned close to the projected values over a broad range of W_t/γ . For stronger bond disorder, fluctuations increase and the long-distance plateau is gradually suppressed, indicating the onset of real singlon population and the breakdown of the projected description.

(iii) *Spin-dependent (magnetic) disorder (Zeeman fields).* We now emphasize a point that is crucial for interpreting the numerics: a random Zeeman field,

$$H_Z = \sum_i (B_i^z S_i^z + B_i^x S_i^x), \quad (43)$$

$$B_i^z, B_i^x \in [-W_Z, W_Z], \quad (44)$$

does not compete with η -pair pumping in our protocol. The reason is structural: the Hubbard model has $SU(2)_S \times SU(2)_\eta$ symmetry, and the two algebras commute, $[S_i^\alpha, \eta_j^\beta] = 0$ for all i, j . Consequently,

$$[H_Z, \eta_i^\pm] = [H_Z, \eta_i^{x,y,z}] = 0, \quad (45)$$

and, even more directly, H_Z acts trivially on the local HD doublet $\{|0\rangle_i, |\uparrow\downarrow\rangle_i\}$ because both states are spin singlets ($\vec{S}_i = 0$). Therefore Zeeman disorder neither breaks the HD closure nor introduces an axis competing with the dissipative $+y$ pinning. In the full microscopic dynamics, H_Z can only enter through higher-order virtual processes together with hopping, which renormalize transients but do not move the attractive fixed point selected by the dissipator. Numerically, we indeed find that the two steady-state diagnostics remain pinned, with $|C_m(r \rightarrow N/2)|_{ss} \rightarrow 1/4$ and $|\Phi_m|_{ss} \rightarrow 1/2$ across the explored field strengths; see Fig. 6.

(iv) *Moderate bond disorder in the Zeno/large- U window.* We finally consider randomness in the kinetic energy,

$$H_{t,\text{dis}} = - \sum_{\langle ij \rangle, \sigma} \delta t_{ij} (c_{i\sigma}^\dagger c_{j\sigma} + \text{H.c.}), \quad \delta t_{ij} \in [t-W_t, t+W_t], \quad (46)$$

which is the most direct microscopic perturbation that promotes processes passing through singly occupied (singlon) configurations. Indeed, a hop starting from a holon–doublon configuration necessarily generates intermediate single occupancies on the two sites involved, so $H_{t,\text{dis}}$ does not preserve the holon–doublon (HD) sector as a strict invariant subspace.

A crucial subtlety, however, is that in the particle-hole symmetric Hubbard setting on a bipartite lattice, bond inhomogeneity of A–B hopping (without frustrating same-sublattice hopping) does not induce coherent dynamics within the η -multiplet: the projected Hamiltonian contribution vanishes, $P[-iH_{\text{Hub}}, \cdot]P = 0$ on $\mathcal{H}_{\Psi} \otimes \mathcal{H}_{\Psi}^*$, and therefore the leading projected generator $\mathcal{L}_{\text{eff}}^{(0)}$ retains the same dark-state structure (Appendix B). Consequently, bond disorder does not tilt the dissipative axis selection inside the reduced manifold in the way that, e.g., angle disorder does.

Bond disorder affects the dynamics instead through the off-manifold blocks in the Schur-complement elimination, PLQ and $Q\mathcal{L}P$, which encode leakage pathways into singlons. Increasing the spread of t_{ij} enhances and spatially inhomogenizes these couplings, thereby strengthening higher-order corrections of the form $-PLQ(Q\mathcal{L}Q)^{-1}Q\mathcal{L}P + \dots$. In the perturbative regime where such excursions remain short-lived (set here by the dissipative separation provided by the driven sites), this mainly reshuffles relaxation pathways and can broaden transient time scales without qualitatively changing the attractor. Consistent with this picture, both $|\Phi_m|_{\text{ss}}$ and the long-distance plateau $|C_m(r \rightarrow N/2)|_{\text{ss}}$ remain close to the projected benchmarks 1/2 and 1/4 over a broad range of W_t (up to finite-size corrections); see Fig. 7.

This robustness is not unlimited. When bond disorder becomes sufficiently strong that hopping-induced excursions are no longer perturbative relative to the dissipative separation scale, real singlon population can accumulate and the projected description begins to break down. Numerically, this crossover shows up as a noticeable suppression of the ODLRO plateau $|C_m(r \rightarrow N/2)|_{\text{ss}}$, typically more pronounced than the reduction of the one-point amplitude $|\Phi_m|_{\text{ss}}$, together with increased sample-to-sample fluctuations at large W_t , as seen in Fig. 7.

B. Disorder that suppresses or destroys the η -pair ODLRO plateau

We now turn to disorders that do affect the steady-state correlators. Operationally, these perturbations either (i) generate a coherent torque within \mathcal{H}_{HD} that competes with the dissipative pinning axis, reducing $|\Phi_m|_{\text{ss}}$ and $|C_m(r \rightarrow N/2)|_{\text{ss}}$, or (ii) open genuinely nonperturbative leakage pathways (e.g. resonant singlon participation or pair-breaking channels) that invalidate the effective pumping picture and drive $|C_m(r \rightarrow N/2)|_{\text{ss}} \rightarrow 0$.

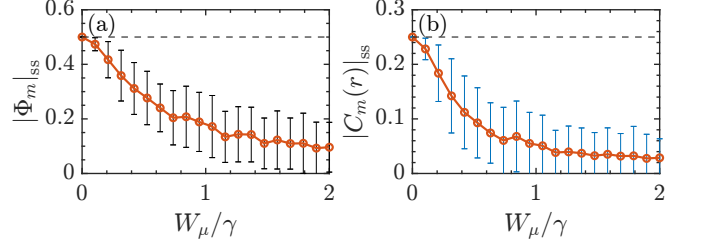


FIG. 8. Response to on-site (chemical-potential) disorder $\mu_i = \mu + \delta\mu_i$ as a function of W_{μ}/γ . (a) $|\Phi_m|_{\text{ss}}$, and (b) $|C_m(r \rightarrow N/2)|_{\text{ss}}$. Parameters: 1D chain with PBC, $t = \gamma$, $U = 6/\gamma$, $\theta = \pi/2$, $N = 5$, and dissipation applied on site 1. Points show disorder averages over 100 realizations; dashed lines mark the projected benchmarks 1/2 and 1/4. In contrast to symmetry-compatible perturbations, on-site inhomogeneity acts as an effective longitudinal field in the η sector and competes with the dissipative phase locking along $+y$. Consistently, both correlators decrease rapidly with increasing W_{μ}/γ , and the long-distance plateau is strongly suppressed at moderate disorder, indicating the breakdown of the projected-manifold picture and the loss of robust ODLRO.

(i) *On-site potential disorder at half filling.* A random scalar potential,

$$H_{\mu} = \sum_i \mu_i (n_{i\uparrow} + n_{i\downarrow} - 1) \quad (47)$$

$$= 2 \sum_i \mu_i \eta_i^z, \quad (48)$$

$$\mu_i \in [-W_{\mu}, W_{\mu}], \quad (49)$$

is qualitatively more dangerous than the previous perturbations because it does not merely broaden decay rates or renormalize phases inside the HD sector: once combined with hopping, it can activate efficient pathways that populate singlons and thereby undermines the mechanism behind the η -pair pumping.

At the level of a single site, H_{μ} acts as a random longitudinal field in the local η -doublet, i.e., it detunes the holon and doublon components through η_i^z . By itself this remains diagonal in the local Fock basis and does not create singlons. The crucial point is that, in the full microscopic Hubbard model, the hopping H_t connects holon/doublon configurations to intermediate singly occupied ones, and the energetic denominators controlling these virtual excursions are set by the local many-body splittings. Potential disorder reshuffles these splittings site by site; consequently, as W_{μ} increases it becomes increasingly likely to find resonant (or near-resonant) local configurations for which the singlon-assisted processes are no longer suppressed by large denominators. In other words, H_{μ} does not directly create singlons, but it substantially enhances the efficiency of singlon-mediated mixing generated by H_t by reducing (and in rare regions, essentially removing) the protection afforded by the interaction gap and/or by the dissipative separation.

From the viewpoint of the effective-generator expansion (Schur-complement elimination), this is precisely the

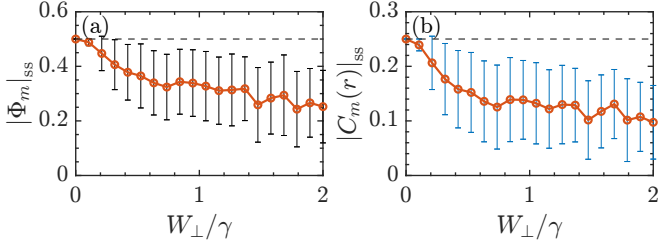


FIG. 9. Response to a random transverse field acting directly in the holon-doublon manifold, $H_\perp = \sum_i (h_i^x \eta_i^x + h_i^y \eta_i^y)$ with $h_i^{x,y} \in [-W_\perp, W_\perp]$, as a function of W_\perp/γ . (a) $|\Phi_m|_{ss}$, and (b) $|C_m(r \rightarrow N/2)|_{ss}$. Parameters: 1D chain with PBC, $t = \gamma$, $U = 6/\gamma$, $\theta = \pi/2$, $N = 5$, and dissipation applied on site 1. Points show disorder averages over 100 realizations; dashed lines mark the projected benchmarks 1/2 and 1/4. Unlike potential disorder, H_\perp is already operative within \mathcal{H}_{HD} : it coherently rotates the local η pseudospin away from the dissipatively selected $+y$ axis. Consistently, both correlators are strongly reduced with increasing W_\perp/γ , demonstrating direct competition with the dissipative phase locking and a rapid suppression of the ODLRO plateau.

regime where the off-manifold resolvent becomes large: the operator $(Q\hat{L}Q)^{-1}$ ceases to be parametrically small because H_μ can pull parts of the Q -sector spectrum toward zero, turning previously higher-order corrections into leading-order contributions. Once this occurs, the rotated dissipation can no longer be viewed as an approximately closed pumping problem within the HD (or η -paired) manifold, and the attractive fixed point is destabilized by real leakage into singlon configurations.

Numerically, this mechanism manifests as a pronounced suppression of both the steady-state one-point amplitude $|\Phi_m|_{ss}$ and the long-distance plateau $|C_m(r \rightarrow N/2)|_{ss}$ with increasing W , and destroying ODLRO; see Fig. 8.

(ii) *Transverse pseudospin fields within \mathcal{H}_{HD} .* A random transverse field acting directly within the holon-doublon manifold,

$$H_\perp = \sum_i (h_i^x \eta_i^x + h_i^y \eta_i^y), \quad (50)$$

$$h_i^x, h_i^y \in [-W_\perp, W_\perp], \quad (51)$$

provides a qualitatively different (and more dangerous) perturbation than potential disorder. While potential disorder becomes destructive mainly by enhancing singlon-mediated leakage once combined with hopping, H_\perp acts already inside \mathcal{H}_{HD} : it coherently rotates the local η pseudospin away from the dissipatively selected $+y$ axis.

Numerically, this competition is immediately visible. As soon as $H_\perp \neq 0$, both $|\Phi_m|_{ss}$ and the long-distance plateau $|C_m(r \rightarrow N/2)|_{ss}$ depart from the projected benchmarks and decrease monotonically with increasing W_\perp [Fig. 9]. In particular, the ODLRO plateau $C_\infty \simeq 1/4$ characteristic of the clean projected theory is lost already at the smallest accessible W_\perp , indicat-

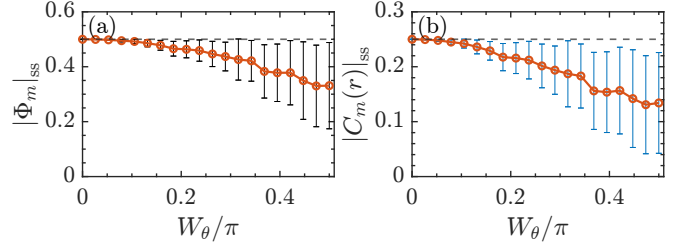


FIG. 10. Response to angle disorder in the rotated dissipation, $\theta_j = \pi/2 + \delta\theta_j$ with $\delta\theta_j \in [-W_\theta, W_\theta]$, as a function of W_θ/π . (a) $|\Phi_m|_{ss}$ and, (b) $|C_m(r \rightarrow N/2)|_{ss}$. Parameters: 1D chain with PBC, $t = \gamma$, $U = 6/\gamma$, nominal rotation $\theta = \pi/2$, $N = 5$, and dissipation applied on site 1. Points show disorder averages over 100 realizations; dashed lines mark the projected benchmarks 1/2 and 1/4. Angle disorder tilts the locally selected dissipative axis: the clean $+y$ dark state is no longer exactly annihilated for $\delta\theta_j \neq 0$, so the attractive fixed point is shifted. Consistent with this, the steady-state correlators remain close to the projected values at weak disorder (small W_θ/π), but are progressively suppressed as W_θ/π increases, with the long-distance correlator $|C_m|_{ss}$ being more sensitive than the one-point amplitude $|\Phi_m|_{ss}$.

ing that the η -paired NESS is not perturbatively stable against transverse fields.

The microscopic reason is simple: the clean protocol relies on dissipative axis selection, i.e., local jumps pin each site toward the $+y$ dark state. A transverse Hamiltonian field continuously generates coherent precession within \mathcal{H}_{HD} , so the dark condition is no longer dynamically preserved and the steady state is pushed away from the $+y$ product fixed point. The resulting NESS becomes a mixed state set by the competition between coherent rotation and dissipative repumping, with strongly reduced long-distance η coherence.

(iii) *Rotation-angle disorder in the jump operators.* Imperfect feedback rotation,

$$L_j = \sqrt{\gamma} \eta_j^- e^{i\theta_j \eta_j^x}, \quad (52)$$

$$\theta_j = \frac{\pi}{2} + \delta\theta_j, \quad \delta\theta_j \in [-W_\theta, W_\theta] \quad (53)$$

is a direct perturbation of the pumping mechanism itself: it rotates the jump away from the ideal $\pi/2$ frame and therefore changes the locally selected dissipative axis. Equivalently, the clean dark state $|\eta_j^y = +1/2\rangle$ is no longer annihilated when $\delta\theta_j \neq 0$. As a consequence, even weak angle disorder immediately shifts the attractive fixed point and the NESS ceases to be the $+y$ product state. In numerics this shows up as a rapid departure of both $|\Phi_m|_{ss}$ and the long-distance plateau $|C_m(r \rightarrow N/2)|_{ss}$ from their projected values as W_θ is increased; see Fig. 10.

(iv) *Pair-breaking noise outside the designed channel.* Finally, we consider additional uncontrolled dissipators that are not aligned with the η -pumping protocol, the

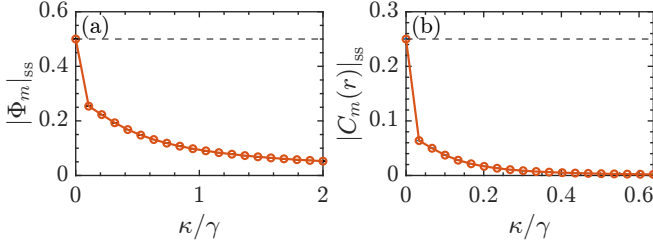


FIG. 11. Pair-breaking single-particle loss with rate κ (normalized as κ/γ) strongly suppresses the η -paired NESS. (a) $|\Phi_m|_{ss}$ and (b) the long-distance plateau $|C_m(r \rightarrow N/2)|_{ss}$ versus κ/γ . Dashed lines indicate the projected benchmarks $1/2$ and $1/4$ at $\kappa = 0$. Parameters: 1D chain with PBC, $t = \gamma$, $U = 6/\gamma$, $\theta = \pi/2$, $N = 5$, and dissipation applied on site 2. Turning on κ induces a leak-and-scramble mechanism: $|C_m(r \rightarrow N/2)|_{ss}$ collapses rapidly toward zero, while $|\Phi_m|_{ss}$ is reduced more gradually due to short-time local repumping but remains bounded by the continuous pair breaking.

most important example being single-particle loss,

$$L_{i\sigma}^{\text{loss}} = \sqrt{\kappa} c_{i\sigma} \quad (54)$$

$$(\text{and similarly dephasing } L_{i\sigma}^{\text{dep}} = \sqrt{\kappa_\phi} n_{i\sigma}). \quad (55)$$

Such channels are qualitatively different from the disorder terms discussed above: they act as genuine pair-breaking processes. In the local Fock basis, $c_{i\sigma}$ converts holons and doublons into singly occupied states,

$$c_{i\sigma} : |0\rangle_i \mapsto 0, \quad |\uparrow\downarrow\rangle_i \mapsto |\bar{\sigma}\rangle_i, \quad c_{i\sigma}^\dagger : |0\rangle_i \mapsto |\sigma\rangle_i, \quad (56)$$

thereby opening real dissipative leakage channels from the holon–doublon doublet span $\{|0\rangle_i, |\uparrow\downarrow\rangle_i\}$ into the singlon sector $\{|\uparrow\rangle_i, |\downarrow\rangle_i\}$. In the η language this is precisely the destruction of the locally pumped coherence: the designed jump $L_j \propto \eta_j^- e^{i\frac{\pi}{2}\eta_j^+}$ can only rephase and repump within the $\eta_j = 1/2$ doublet, whereas single-particle loss continuously removes weight from that sector and scrambles the relative phase between $|0\rangle_i$ and $|\uparrow\downarrow\rangle_i$.

Numerically, this leak-and-scramble channel is strongly detrimental to η -pair coherence. As soon as the loss rate κ is nonzero, the long-distance correlator $|C_m(r \rightarrow N/2)|_{ss}$ is rapidly suppressed toward zero, signaling a prompt destruction of ODLRO; see Fig. 11. The one-point amplitude $|\Phi_m|_{ss}$ is also reduced, typically more gradually, because local rotated pumping can transiently repolarize the η pseudospin and sustain short-range coherence, but it cannot compensate an ongoing pair-breaking process at long times. In this sense, uncontrolled loss imposes a stringent upper bound on the steady-state ODLRO plateau and, for fixed pumping strength γ , sets the achievable quality (and effective lifetime) of the η -paired nonequilibrium steady state.

In summary, the disorder response supports a symmetry-based robustness principle: perturbations that are diagonal (or effectively longitudinal) in the local HD doublet mainly renormalize relaxation pathways and leave the ODLRO plateau close to the projected value,

whereas perturbations that (i) compete directly with the dissipative axis selection (e.g., transverse fields or angle disorder) or (ii) open real leakage/pair-breaking channels (e.g., single-particle loss) suppress and ultimately destroy the nonequilibrium superconducting order.

VI. CONCLUSION AND OUTLOOK

We have demonstrated that superconducting-like order can be stabilized as a nonequilibrium attractor in a strongly correlated lattice system. For the particle-hole symmetric Hubbard chain, we introduced a rotated quantum-jump protocol based on a locally rotated η -pair lowering operator and showed that the Lindblad dynamics converges from the vacuum to a NESS with η -pair ODLRO.

The mechanism underlying our protocol can be understood through three essential components. First, local dark-state engineering: the rotated quantum jump operator reshapes the local dark-state manifold and imprints a well-defined η -pseudospin phase, thereby establishing a robust on-site coherence between holon and doublon configurations. Second, selective pumping governed by the representation structure of the dissipator and dynamical separation of timescales: since the local η operators act nontrivially only within the holon–doublon doublet while annihilating singlon states, the dissipative dynamics does not directly generate singly occupied configurations. Any singlon admixture originates solely from coherent hopping processes and remains perturbative in the regime where fast dynamical components can be systematically eliminated via a controlled Schur-complement expansion. Third, coherence propagation mediated by coherent hopping together with Liouvillian selection: the imprinted pseudospin phase spreads across the lattice through coherent dynamics, while the projected Liouvillian dynamics selects the η -paired subspace as an attractive manifold and opens a dissipative gap that governs the relaxation timescale toward the steady state. A notable consequence of this mechanism is a local-to-global preparation principle: dissipative action confined to a single lattice site can induce macroscopic ODLRO throughout the interacting many-body system.

We further established that this η -paired NESS is robust against broad classes of static disorder, which mainly renormalize transient dynamics and relaxation rates, and we identified specific perturbations that directly compete with dissipative axis selection (or introduce pair breaking) and thus suppress long-range order. Looking forward, several directions are immediately suggested. First, it would be valuable to develop analytic scaling descriptions of the dissipative gap and relaxation with system size, driving geometry, and disorder strength. Second, the mechanism is not tied to one dimension: since η -SU(2) structure and the staggered η -pair generators are naturally compatible with any bipartite lattice, the protocol should extend directly to arbit-

trary bipartite geometries (and, in particular, to higher-dimensional lattices) with appropriate choices of driven sites. Third, spatially patterned or time-dependent rotations/jumps offer a natural route to imprint phase textures, domain structures, and supercurrents in a controlled manner. More broadly, our results illustrate a local-to-global preparation principle: minimal, local dissipation engineering can autonomously stabilize superconducting order as an attractor of strongly correlated open-system dynamics.

ACKNOWLEDGMENTS

We acknowledge the support of the National Natural Science Foundation of China under Grants No. 12275193 and 11975166.

Appendix A: Explicit Liouvillian matrix for the single-qubit example

In this Appendix we present the explicit matrix representation of the Liouvillian for the single-qubit models in Sec. II. We employ the standard vectorization identity $\text{vec}(A\rho B) = (A \otimes B^T)\text{vec}(\rho)$, under which

$$\mathcal{L} = (L \otimes L^*) - \frac{1}{2}(L^\dagger L \otimes \mathbb{I}) - \frac{1}{2}(\mathbb{I} \otimes (L^\dagger L)^T), \quad (\text{A1})$$

where $H = 0$ has been used.

We work in the z -basis $\{|\uparrow\rangle, |\downarrow\rangle\}$ with

$$s^x = \frac{1}{2} \begin{pmatrix} 0 & 1 \\ 1 & 0 \end{pmatrix}, \quad s^y = \frac{1}{2} \begin{pmatrix} 0 & -i \\ i & 0 \end{pmatrix}, \quad s^- = \begin{pmatrix} 0 & 0 \\ 1 & 0 \end{pmatrix}. \quad (\text{A2})$$

We choose the ordering $\text{vec}(\rho) = (\rho_{\uparrow\uparrow}, \rho_{\uparrow\downarrow}, \rho_{\downarrow\uparrow}, \rho_{\downarrow\downarrow})^T$.

For the rotated jump $L(\theta) = \sqrt{\gamma} s^- e^{i\theta s^x}$, the case $\theta = \pi/2$ yields

$$s^- e^{i\frac{\pi}{2}s^x} = \frac{\sqrt{2}}{2} \begin{pmatrix} 0 & 0 \\ 1 & i \end{pmatrix}, \quad (\text{A3})$$

and Eq. A1 gives the explicit 4×4 Liouvillian matrix

$$\mathcal{L}_{\pi/2} = \gamma \begin{pmatrix} -\frac{1}{2} & \frac{i}{4} & -\frac{i}{4} & 0 \\ -\frac{i}{4} & -\frac{1}{2} & 0 & -\frac{i}{4} \\ \frac{i}{4} & 0 & -\frac{1}{2} & \frac{i}{4} \\ \frac{1}{2} & -\frac{i}{4} & \frac{i}{4} & 0 \end{pmatrix}. \quad (\text{A4})$$

Its spectrum contains a unique mode with $\text{Re}(\lambda) = 0$ (indeed $\lambda = 0$), which determines the steady state. Solving $\mathcal{L}_{\pi/2} \text{vec}(\rho_{\text{ss}}) = 0$ yields

$$\text{vec}(\rho_{\text{ss}}) \propto \begin{pmatrix} 1 \\ -i \\ i \\ 1 \end{pmatrix}, \quad \rho_{\text{ss}} \propto \begin{pmatrix} 1 & -i \\ i & 1 \end{pmatrix} = 2 |\psi_d(\frac{\pi}{2})\rangle \langle \psi_d(\frac{\pi}{2})|, \quad (\text{A5})$$

which is consistent with the pure dark state in Eq. 5.

Appendix B: Derivation of the projected effective Liouvillian from Feshbach (Schur-complement) elimination

This appendix derives the projected generator Eq. (22) starting from the microscopic Lindblad equation (14). Our goal is twofold: (i) to obtain the leading effective Liouvillian acting within the chosen slow manifold, and (ii) to record a systematic organization of higher-order corrections via the Feshbach (Schur-complement) map.

1. Feshbach map for a Liouvillian superoperator

We consider the vectorized form of the Lindblad generator, viewed as a linear operator $\hat{\mathcal{L}}$ acting on the doubled space $\mathcal{H} \otimes \mathcal{H}^*$. Let P be the projector onto the selected slow manifold \mathcal{M} (in the main text, the doubled manifold relevant to the η -pairing discussion), and $Q = \mathbb{I} - P$ be the complementary projector. Writing the eigenproblem

$$\hat{\mathcal{L}} |x\rangle = \lambda |x\rangle \quad (\text{B1})$$

in the block form with respect to $P \oplus Q$, one obtains the exact Feshbach map

$$\hat{\mathcal{L}}_{\text{eff}}(\lambda) = P \hat{\mathcal{L}} P + P \hat{\mathcal{L}} Q (\lambda - Q \hat{\mathcal{L}} Q)^{-1} Q \hat{\mathcal{L}} P, \quad (\text{B2})$$

whenever $(\lambda - Q \hat{\mathcal{L}} Q)$ is invertible on $Q(\mathcal{H} \otimes \mathcal{H}^*)$. For the steady-state problem one sets $\lambda = 0$, yielding the standard expansion

$$\hat{\mathcal{L}}_{\text{eff}} = P \hat{\mathcal{L}} P - P \hat{\mathcal{L}} Q (Q \hat{\mathcal{L}} Q)^{-1} Q \hat{\mathcal{L}} P + \dots, \quad (\text{B3})$$

where the ellipsis denotes higher-order contributions (and, if $Q \hat{\mathcal{L}} Q$ has a kernel, the inverse is understood as an appropriate pseudo-inverse). Equation (B3) provides the systematic meaning of the leading projected generator $P \hat{\mathcal{L}} P$ used in Sec. III: it captures the dominant attractive fixed point and the primary dissipative gap, while the subleading Schur-complement term encodes perturbative excursions out of \mathcal{M} .

2. Vectorization and ket \otimes bra representation

Under the Choi–Jamiolkowski isomorphism, the density matrix is mapped to a vector $|\rho\rangle \in \mathcal{H} \otimes \mathcal{H}^*$ such that left (right) multiplication becomes an operator acting on the ket (bra) factor. The microscopic Lindbladian (14) is represented by the non-Hermitian operator

$$\begin{aligned} \hat{\mathcal{L}} = & -i (H_{\text{Hub}} \otimes \mathbb{I} - \mathbb{I} \otimes H_{\text{Hub}}^T) \\ & + \sum_{j \in \mathcal{J}} \left(L_j \otimes L_j^* - \frac{1}{2} L_j^\dagger L_j \otimes \mathbb{I} - \frac{1}{2} \mathbb{I} \otimes L_j^T L_j^* \right). \end{aligned} \quad (\text{B4})$$

In the main text we choose \mathcal{M} such that, within $P(\mathcal{H} \otimes \mathcal{H}^*)$, the coherent part does not contribute:

$$P [-i (H_{\text{Hub}} \otimes \mathbb{I} - \mathbb{I} \otimes H_{\text{Hub}}^T)] P = 0, \quad (\text{B5})$$

which follows from the properties of H_{Hub} on the chosen manifold (see Sec. III). Hence the leading projected generator $P\hat{\mathcal{L}}P$ is governed purely by the dissipators. We take the rotated jump operator

$$L_j = \sqrt{\gamma} \eta_j^- e^{i\frac{\pi}{2}\eta_j^x}. \quad (\text{B6})$$

Within the local holon–doublon doublet (a spin-1/2 representation of η_j), one has the identity

$$\eta_j^+ \eta_j^- = \frac{1}{2} - \eta_j^z. \quad (\text{B7})$$

Therefore

$$L_j^\dagger L_j = \gamma e^{-i\frac{\pi}{2}\eta_j^x} \eta_j^+ \eta_j^- e^{i\frac{\pi}{2}\eta_j^x} = \gamma e^{-i\frac{\pi}{2}\eta_j^x} \left(\frac{1}{2} - \eta_j^z \right) e^{i\frac{\pi}{2}\eta_j^x}.$$

Using the rotation identity

$$e^{-i\frac{\pi}{2}\eta_j^x} \eta_j^z e^{i\frac{\pi}{2}\eta_j^x} = -\eta_j^y, \quad (\text{B8})$$

we obtain the compact form

$$L_j^\dagger L_j = \frac{\gamma}{2} - \gamma \eta_j^y. \quad (\text{B9})$$

3. Leading projected generator $P\hat{\mathcal{L}}P$ and Eq. (22)

Substituting Eq. (B9) into Eq. (B4), and denoting operators acting on the bra factor by tildes, the anticommutator terms become

$$-\frac{1}{2} L_j^\dagger L_j \otimes \mathbb{I} - \frac{1}{2} \mathbb{I} \otimes L_j^T L_j^* = -\frac{\gamma}{2} \mathbb{I} + \frac{\gamma}{2} (\eta_j^y - \tilde{\eta}_j^y). \quad (\text{B10})$$

The relative sign between η_j^y and $\tilde{\eta}_j^y$ follows from $\eta^{y*} = -\eta^y$ in the standard representation (while $\eta^{x*} = \eta^x$). The recycling term reads

$$L_j \otimes L_j^* = \gamma \left(\eta_j^- e^{i\frac{\pi}{2}\eta_j^x} \right) \left(\tilde{\eta}_j^- e^{-i\frac{\pi}{2}\tilde{\eta}_j^x} \right), \quad (\text{B11})$$

which couples the ket and bra factors locally. Summing over driven sites $j \in \mathcal{J}$ and restricting to the leading projected generator yields

$$\begin{aligned} \hat{\mathcal{L}}_{\text{eff}}^{(0)} &\equiv P\hat{\mathcal{L}}P \\ &= -\frac{\gamma|\mathcal{J}|}{2} + \gamma \sum_{j \in \mathcal{J}} \left[\frac{1}{2} (\eta_j^y - \tilde{\eta}_j^y) + \eta_j^- e^{i\frac{\pi}{2}\eta_j^x} \tilde{\eta}_j^- e^{-i\frac{\pi}{2}\tilde{\eta}_j^x} \right] \end{aligned} \quad (\text{B12})$$

which is Eq. (22) in the main text. The next term in Eq. (B3),

$$-P\hat{\mathcal{L}}Q(Q\hat{\mathcal{L}}Q)^{-1}Q\hat{\mathcal{L}}P, \quad (\text{B14})$$

organizes higher-order excursions out of \mathcal{M} and back. In our context these excursions include (i) mixing among different global- η sectors within holon–doublon space induced by the locality of L_j , and (ii) virtual leakage processes mediated primarily by the hopping H_t that temporarily populate singly occupied configurations. Equation (B14) provides the controlled bookkeeping for how such processes renormalize transient relaxation pathways and shift nonzero decay modes, while the leading attractive fixed point captured by $P\hat{\mathcal{L}}P$ remains the dominant organizing principle in the regime studied.

Appendix C: Proof of the strictly upper-triangular form of $\hat{\mathcal{L}}$ in the η^y basis

In this Appendix we prove the statement used in the main text: within the η -pairing manifold, the operator $\hat{\mathcal{L}}$ in Eq. (22) admits a strictly upper-triangular matrix representation in the doubled-space basis where η_j^y and $\tilde{\eta}_j^y$ are diagonal. As a consequence, the spectrum is given exactly by the diagonal part, leading to Eq. (22) and the universal gap $\Delta = \gamma/2$.

1. Single-site lemma: $K = \eta^- e^{i\frac{\pi}{2}\eta^x}$ is upper triangular in the η^y basis

On a single site, the local pseudospin is a spin-1/2 representation of $SU(2)$. Let $\{|+y\rangle, |-y\rangle\}$ denote the eigenstates of η^y ,

$$\eta^y |\pm y\rangle = \pm \frac{1}{2} |\pm y\rangle, \quad \langle +y| -y \rangle = 0, \quad (\text{C1})$$

and order the basis as $\{|+y\rangle, |-y\rangle\}$ (descending m_y). Define the rotated lowering operator

$$K \equiv \eta^- e^{i\frac{\pi}{2}\eta^x}. \quad (\text{C2})$$

We claim that K has the strictly upper-triangular form

$$K^{(y)} = \begin{pmatrix} 0 & -i\frac{\sqrt{2}}{2} \\ 0 & i\frac{\sqrt{2}}{2} \end{pmatrix} \quad \text{in the ordered basis } \{|+y\rangle, |-y\rangle\}. \quad (\text{C3})$$

To prove this, it suffices to show that K annihilates the $+y$ eigenstate. Let $U \equiv e^{-i\frac{\pi}{2}\eta^x}$ so that $K = U^\dagger \eta^- U$. Then $K|+y\rangle = 0$ is equivalent to $\eta^- U|+y\rangle = 0$. Since η^- annihilates the lowest-weight state in the z -quantization, the condition $\eta^- |\phi\rangle = 0$ implies $|\phi\rangle \propto |\downarrow_z\rangle$. But U is precisely the rotation mapping $|+y\rangle$ to $|\downarrow_z\rangle$, hence

$$K|+y\rangle = \eta^- e^{i\frac{\pi}{2}\eta^x} |+y\rangle = 0. \quad (\text{C4})$$

Equation (C4) implies that the first column of $K^{(y)}$ vanishes:

$$\langle +y|K|+y\rangle = 0, \quad \langle -y|K|+y\rangle = 0, \quad (\text{C5})$$

which proves Eq. (C3). Therefore K is strictly upper triangular in the η^y basis.

2. Doubled-space ordering and triangularity of the jump term

We now consider the doubled-space basis used in the main text, where each η_j^y and $\tilde{\eta}_j^y$ is diagonal. A convenient product basis is labeled by the local eigenvalues

$$\eta_j^y |m_j\rangle = m_j |m_j\rangle, \quad \tilde{\eta}_j^y |\tilde{m}_j\rangle = \tilde{m}_j |\tilde{m}_j\rangle, \quad m_j, \tilde{m}_j = \pm \frac{1}{2}. \quad (\text{C6})$$

We define the doubled basis vectors as

$$|\{m_j, \tilde{m}_j\}\rangle\rangle \equiv \bigotimes_{j=1}^N |m_j\rangle \otimes |\tilde{m}_j\rangle, \quad (\text{C7})$$

and order them lexicographically with m_j and \tilde{m}_j both ordered as $(+\frac{1}{2}) \succ (-\frac{1}{2})$ at each site.

Within this ordering, the diagonal operator

$$D_j \equiv \frac{1}{2} (\eta_j^y - \tilde{\eta}_j^y) \quad (\text{C8})$$

is manifestly diagonal, while the ket–bra coupling term in Eq. (22) is

$$J_j \equiv \eta_j^- e^{i\frac{\pi}{2}\eta_j^x} \tilde{\eta}_j^- e^{-i\frac{\pi}{2}\tilde{\eta}_j^x} = K_j \tilde{K}_j, \quad (\text{C9})$$

where K_j and \tilde{K}_j act on the ket and bra degrees of freedom at site j , respectively. By the single-site lemma above, both K_j and \tilde{K}_j are strictly upper triangular in their local η^y eigenbases. Therefore the product $J_j = K_j \tilde{K}_j$ is also strictly upper triangular on the local doubled space at site j , and hence cannot contribute to any diagonal matrix element in the global doubled basis.

It follows that the full operator $\hat{\mathcal{L}}_{\text{eff}}^{(0)}$ in Eq. (22), being a sum of diagonal terms and strictly upper-triangular

terms (in the above ordering), is itself strictly upper triangular up to the diagonal part. In particular, the eigenvalues of $\hat{\mathcal{L}}_{\text{eff}}^{(0)}$ are exactly given by its diagonal entries, i.e.,

$$\lambda_{\{m_j, \tilde{m}_j\}} = \sum_{j \in \mathcal{J}} \left[-\frac{\gamma}{2} + \gamma \langle \{m, \tilde{m}\} | D_j | \{m, \tilde{m}\} \rangle \right] \quad (\text{C10})$$

$$= \sum_{j \in \mathcal{J}} \left[-\frac{\gamma}{2} + \frac{\gamma}{2} (m_j - \tilde{m}_j) \right], \quad (\text{C11})$$

which is Eq. (26) of the main text.

3. Minimal explicit example: one driven site

For completeness, consider one driven site (drop the site index) and the local doubled basis $\{|+y\rangle \otimes |+y\rangle, |+y\rangle \otimes |-y\rangle, |-y\rangle \otimes |+y\rangle, |-y\rangle \otimes |-y\rangle\}$. In this basis, the diagonal contribution is

$$-\frac{\gamma}{2} + \frac{\gamma}{2} (\eta^y - \tilde{\eta}^y) = \text{diag} \left(-\frac{\gamma}{2}, 0, -\gamma, -\frac{\gamma}{2} \right), \quad (\text{C12})$$

while the jump term $J = K \tilde{K}$ is strictly upper triangular and thus leaves the diagonal entries unchanged. Hence the diagonal part fully determines the eigenvalues, and the smallest nonzero decay rate is $\gamma/2$, establishing the Liouvillian gap $\Delta = \gamma/2$.

[1] G. Lindblad, Communications in Mathematical Physics **48**, 119 (1976).

[2] V. Gorini, A. Kossakowski, and E. C. G. Sudarshan, Journal of Mathematical Physics **17**, 821 (1976).

[3] H.-P. Breuer and F. Petruccione, *The Theory of Open Quantum Systems* (Oxford University Press, Oxford, 2002).

[4] J. Dalibard, Y. Castin, and K. Mølmer, Phys. Rev. Lett. **68**, 580 (1992).

[5] J. F. Poyatos, J. I. Cirac, and P. Zoller, Phys. Rev. Lett. **77**, 4728 (1996).

[6] B. Kraus, H. P. Büchler, S. Diehl, A. Kantian, A. Micheli, and P. Zoller, Phys. Rev. A **78**, 042307 (2008).

[7] F. Verstraete, M. M. Wolf, and J. I. Cirac, Nat. Phys. **5**, 633 (2009).

[8] M. Müller, K. Hammerer, Y. Zhou, C. F. Roos, and P. Zoller, Advances In Atomic, Molecular, and Optical Physics **61**, 1 (2012).

[9] A. J. Daley, Advances in Physics **63**, 77 (2014).

[10] L. M. Sieberer, M. Büchhold, and S. Diehl, Rep. Prog. Phys. **79**, 096001 (2016).

[11] L. M. Sieberer, M. Büchhold, J. Marino, and S. Diehl, Rev. Mod. Phys. **97**, 025004 (2025).

[12] F. Minganti, A. Biella, N. Bartolo, and C. Ciuti, Phys. Rev. A **98**, 042118 (2018).

[13] X. Z. Zhang, Phys. Rev. B **109**, 184314 (2024).

[14] M. J. Kastoryano, F. Reiter, and A. S. Sørensen, Phys. Rev. Lett. **106**, 090502 (2011).

[15] J. T. Barreiro, M. Müller, P. Schindler, D. Nigg, T. Monz, M. Chwalla, M. Hennrich, C. F. Roos, P. Zoller, and R. Blatt, Nature **470**, 486 (2011).

[16] S. Shankar, M. Hatridge, Z. Leghtas, K. M. Sliwa, A. Narla, U. Vool, S. M. Girvin, L. Frunzio, M. Mirrahimi, and M. H. Devoret, Nature **504**, 419 (2013).

[17] S. Diehl, E. Rico, M. A. Baranov, and P. Zoller, Nat. Phys. **7**, 971 (2011).

[18] C.-E. Bardyn, M. A. Baranov, E. Rico, A. İmamoğlu, P. Zoller, and S. Diehl, Phys. Rev. Lett. **109**, 130402 (2012).

[19] F. Iemini, D. Rossini, R. Fazio, S. Diehl, and L. Mazza, Phys. Rev. B **93**, 115113 (2016).

[20] M. Goldstein, SciPost Physics **7**, 067 (2019).

[21] S. Diehl, A. Micheli, A. Kantian, B. Kraus, H. P. Büchler, and P. Zoller, Nat. Phys. **4**, 878 (2008).

[22] S. Diehl, W. Yi, A. J. Daley, and P. Zoller, Phys. Rev. Lett. **105**, 227001 (2010).

[23] I. Carusotto and C. Ciuti, Rev. Mod. Phys. **85**, 299 (2013).

[24] C. N. Yang, Phys. Rev. Lett. **63**, 2144 (1989).

[25] J. Tindall, B. Buča, J. R. Coulthard, and D. Jaksch, Phys. Rev. Lett. **123**, 030603 (2019).

[26] D. K. Mark and O. I. Motrunich, Phys. Rev. B **102**, 075132 (2020).

[27] J.-S. Bernier, L. Tan, U. Schollwöck, and C. Kollath, Phys. Rev. B **98**, 144519 (2018).

- [28] B. Buča, J. Tindall, and D. Jaksch, *Nat. Commun.* **10**, 1730 (2019).
- [29] V. V. Albert and L. Jiang, *Phys. Rev. A* **89**, 022118 (2014).
- [30] B. Buča and T. Prosen, *New J. Phys.* **14**, 073007 (2012).
- [31] M. Žnidarič and M. Horvat, *Eur. Phys. J. B* **86**, 67 (2013).
- [32] G. Beaulieu, F. Minganti, S. Frasca, S. Felicetti, R. Di Candia, V. Savona, and P. Scarlino, *Nat. Commun.* **16**, 1954 (2025).